Effect of Growth Rates and Temperature Gradients on the Spacing and Undercooling in the Broken-Lamellar Eutectic Growth (Sn-Zn Eutectic System)

H. Kaya, E. Çadırlı, and M. Gündüz

(Submitted 18 February 2003)

The Sn-Zn system has a eutectic structure of a broken lamellar type. Dependence of the broken-lamellar spacing λ and the undercooling ΔT on V and G were investigated, and the relationship between them was examined. A Sn-Zn (99.99%) high-purity eutectic alloy was melted in a graphite crucible under vacuum atmosphere. This eutectic alloy was directionally solidified upward with a constant growth rate V (8.30 μm/s) and different temperature gradients G (1.86-6.52 K/mm), and also with a constant temperature gradient (6.52 K/mm) and different growth rates (8.30-165.13 μm/s) in a Bridgman-type directional solidification furnace. The lamellar spacings λ were measured from both transverse and longitudinal sections of the specimen. The λ values from the transverse section were used for calculations and comparisons with the previous works. The undercooling values ΔT were obtained using growth rate and system parameters K_1 and K_2. It was found that the values of λ decreased while V and G increased. The relationships between lamellar spacing λ and solidification parameters V and G were obtained by linear regression analysis method. The $\lambda^2 V$, $\Delta T\lambda$, $\Delta T V^{-0.5}$, and $\lambda^3 G$ values were determined using λ, ΔT, V, and G values. The experimentally obtained values for the broken-lamellar growth (Sn-Zn eutectic system) were in good agreement with the theoretical and other experimental values.

Keywords broken-lamellar growth, directional solidification, eutectic alloys, lamellar spacings, Sn-Zn eutectic alloys, undercooling, microstructure

1. Introduction

Eutectic alloys are the basis of most casting alloys. In the 1960s, directional solidification was developed to process eutectic alloys.[1-5] Research initially focused on materials for high-temperature structural applications, but it was soon broadened to non-structural materials for electronic, magnetic, and optical applications.[6]

The vast majority of technically important eutectic alloys is composed of two phases. Directional solidification of binary or pseudo-binary eutectics may result in regular structures of fibrous or lamellar type. In fibrous growth, one of the phases grows in the form of fibers embedded into a continuous matrix of the other phase, while in the case of lamellar growth, two phases grow cooperatively side by side in the form of lamellae or broken lamellae. Lamellae or broken-lamellae growth from the melt occurs when the solidification of eutectic melts simultaneously produces two distinct solid phases (α and β phases).

H. Kaya and **E. Çadırlı,** Niğde University, Faculty of Arts and Sciences, Department of Physics, Niğde, Turkey; and **M. Gündüz,** Erciyes University, Faculty of Arts and Sciences, Department of Physics, Kayseri, Turkey. Contact e-mail: gunduz@erciyes.edu.tr.

On the basis of the classification suggested by Crocker et al.[7] and Elliot,[8] the Sn-Zn eutectic system has a eutectic structure of the broken-lamellar type, the volume fraction of faceted lamellar phase being 8.3% and the other being non-faceted.[7] These types of microstructures have many fault lines. The formation of a fault is attributed to the dynamics of a local spacing selection. However, the mechanism for spacing selection is not fully understood.[9]

In the form of the lamellae process, the solid/liquid interface is formed from alternating solid phases in contact with the eutectic melt. The way a lamellar eutectic grows depends on mass transport at the solid/liquid interface. Since solid phases arise from the cross-diffusion of solute in the interfacial liquid, change in the growth rate, thermal gradient at the interface, convection in the melt, and purity of the eutectic alloy directly influence the morphology of the eutectic microstructure.[10] In recent decades, many physicists and metallurgists have attempted to obtain supercooling ΔT and lamellar spacing λ as functions of growth rate V and temperature gradient G, respectively.[9-22]

One of the most significant theoretical studies is the Jackson and Hunt (J-H) model[11] of the regular lamellar eutectic structure. At the extremum condition, J-H obtained the relationships between λ, V, and ΔT as

$$\Delta T = K_1 V \lambda + K_2/\lambda \quad \text{(Eq 1)}$$

$$\lambda_e^2 V = K_2/K_1 \quad \text{(Eq 2a)}$$

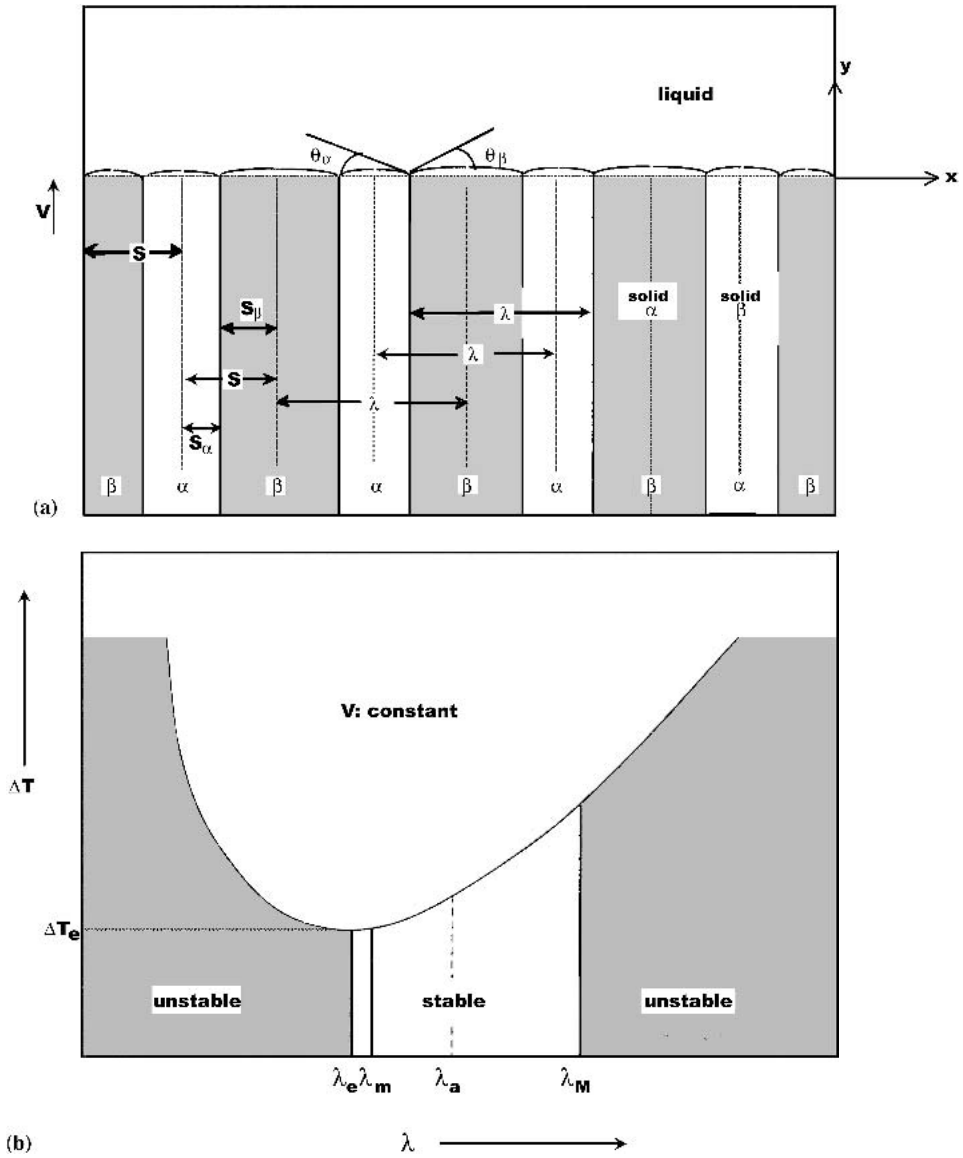

Fig. 1 **(a)** Schematic representation of regular eutectics, which defines the coordinate system and the contact angle at the triple point junctions; **(b)** growth equation showing the variation of undercooling with interlamellar spacing at constant growth velocity and defining the steady state range of lamellar growth, spacings

$$\Delta T_e \lambda_e = 2 K_2 \quad \text{(Eq 2b)}$$

$$\frac{\Delta T_e^2}{V} = 4 K_1 K_2 \quad \text{(Eq 2c)}$$

where ΔT_e is the minimum interface undercooling and K_1 and K_2 can be evaluated from phase diagram and thermodynamic data. They are given by

$$K_1 = mPC_0/f_\alpha/f_\beta D \quad \text{(Eq 3)}$$

and

$$K_2 = 2m\delta \sum_i (\Gamma_i \sin \theta_i / m_i f_i);\ i = \alpha, \beta \quad \text{(Eq 4)}$$

where $m = m_\alpha m_\beta/(m_\alpha + m_\beta)$ in which m_α and m_β are the slopes of the liquidus lines of the α and β phases at the eutectic temperature, C_o is the difference between the composition in the β and the α phase, f_α and f_β are the volume fractions of α and β phases, respectively. Γ_i is the Gibbs-Thompson coefficient, D is solute diffusion coefficient for the melt, and θ_α and θ_β are the groove angles of α/liquid phases and β/liquid phases at the three-phase conjunction point (Fig. 1a). These parameters concerning Zn-Sn eutectic alloy are given in Appendix A. The parameter δ is unity for the lamellar growth. For lamellar eutectic the parameter P (Peclet number) is defined as[11]

$$P = 0.3383 (f_\alpha f_\beta)^{1.661} \quad \text{(Eq 5)}$$

A well-known conjecture of this criterion is the minimum supercooling argument.[23] This indicates that the spacing λ, as indicated in Fig.1(b), will be the operating point of spacing selection.[11] Analysis of the stability of the solidifying interface shows that this argument coincides with the marginal stability principle.[18,19]

Recently, a series of precise measurements on the CBr_4-C_2Cl_6 system,[24] lead-based alloys,[25] and a few other systems[26] in directional solidification showed the existence of a selection band of spacings.[24-26] In fact, the J-H eutectic theory[11] also predicted a stable range of spacing selection, within which the solidifying interface was argued to propagate stably, as indicated in Fig.1b. The lower limit λ_m of this range corresponds to the minimum supercooling arguments, whereas the upper limit λ_M corresponds to the value where the solidifying interface of the larger volume fraction phase requires an infinite slope. Naturally, the minimum supercooling argument should be superior to the other spacings to be selected. So far, the published experimental data for the band fall into the stable range predicted by the J-H theory.[24-26] Although the measured lower limit λ_m of the band is roughly consistent with λ, the measured upper limit λ_M is much lower than the absolute destabilization limit $\lambda_{M,}$ as shown in Fig.1(b).

The existence of the selection band of spacings predicts that there should be at least two operating points of spacing selection for a eutectic system. The J-H eutectic theory[11] obviously overestimates the upper limit of selection band. The maximum spacing λ_M is limited by the motion of lamellar faults. Consequently, the eutectic growth at constant growth rate occurs within a small range of spacing values, near the extremum spacing. Therefore, the value of $\lambda_{e,}$ λ_a, λ_m, and λ_M was measured based on J-H criterion both on the longitudinal and on the transverse sections for this alloy system.

In directional solidification experiments both *V* and *G* can be independently controlled, so that one may study the dependence of λ on either *V* at a constant *G* (case 1) or *G* at a constant *V* (case 2). Many studies have been done to determine experimentally the dependence of structure parameter, lamellar spacing λ, on solidification parameters, growth rate *V*, and temperature gradient *G* in the directional solidification experiments.[14, 24-43] These studies have shown that λ decreases as *V* and *G* increase. The lamellar spacing λ can be expressed for the case 1 as

$$\lambda = k_1 V^{-m} \quad \text{(Eq 6)}$$

where k_1 is a constant. The lamellar spacing λ can be expressed for the case 2 as

$$\lambda = k_2 G^{-n} \quad \text{(Eq 7)}$$

where k_2 is a constant. As can be seen from Eq 7, λ decreases with increasing *G* values.

In this work the binary eutectic Sn-Zn system, which has a broken-lamellar structure, was directionally solidified upward under the argon atmosphere to determine the dependence of broken-lamellar spacing λ on *V*, *G*, and Δ*T*, and to compare the results with eutectic theory[11] and previous experimental studies.

2. Experimental Details

The samples were prepared by melting together appropriate amounts of tin and zinc (both of 99.99% purity) in a vacuum melting furnace.[44] After allowing time for melt homogenization, molten alloy was poured into the thirteen graphite crucibles [4 mm inner diameter (ID), 6.35 mm outer diameter (OD), and 250 mm in length (L)], which were placed in the hot filling furnace,[44] and then the samples were solidified. The specimens were grown by being withdrawn from a two-zone vertical Bridgman-type resistance heated furnace (details of the directional solidification furnace are presented in Ref. 45). To prevent the sample from oxidizing, argon gas was continuously introduced into the graphite crucible during solidification. When the growth length extended to about 100 mm, the sample was water quenched to observe the solid-liquid interface.

2.1 Measurement of the Growth Rates, the Temperature Gradients and Calculation of the Undercooling

Temperature of the Bridgman furnace was controlled by a Pt/Pt-%13 Rh thermocouple placed between the heating element and the alumina tube. The sample was placed in a graphite cylinder (ID = 10 mm, OD = 40 mm, L = 300 mm) to obtain a uniform temperature (experimental details are given in Ref. 32 and 33). Temperatures were measured with three alumel/chromel thermocouples positioned vertically 10 mm apart from each other and parallel to the heat flow direction. The thermocouples positioned into 0.8 mm ID, 1.2 mm OD alumina sheaths. All the thermocouple leads were taken to a constant cold junction and then to a thermally insulated switch by means of which each thermocouple could be introduced in turn to a further circuit consisting of a constant voltage supply acting as a backing off unit and a Kipp and Zonen (Kipp & Zonen Inc., Saskatoon, Canada) recorder capable of recording to 1 μV or 0.025 K. Eutectic temperatures were measured from the heating and cooling curves. It was observed that the melting point of eutectic is 471.5 K (198.5 °C), which is good agreement with previous work.[46] The values were calculated for the growth velocity from measurements of the time taken for the interface to pass successive thermocouples separated by a known distance. The average value was used for the growth velocity.

When the second thermocouple at the solid-liquid interface temperature (T_E) and third thermocouple in the liquid were recorded simultaneously for measurement of *G* on the solid-liquid interface, Δ*T*-λ curves were obtained by using measured *V* and λ values, and the extremum undercooling values ΔT_e were calculated from Eq 2c.

To obtain the undercoolings from Eq 1, K_1 and K_2 system parameters were calculated from Eq 3, 4, and 5 by using the physical constant of Sn-Zn eutectic alloy (Appendix A). K_1 and K_2 values were 0.0070 (K s /μm^2) and 0.260 (K μm), respectively.

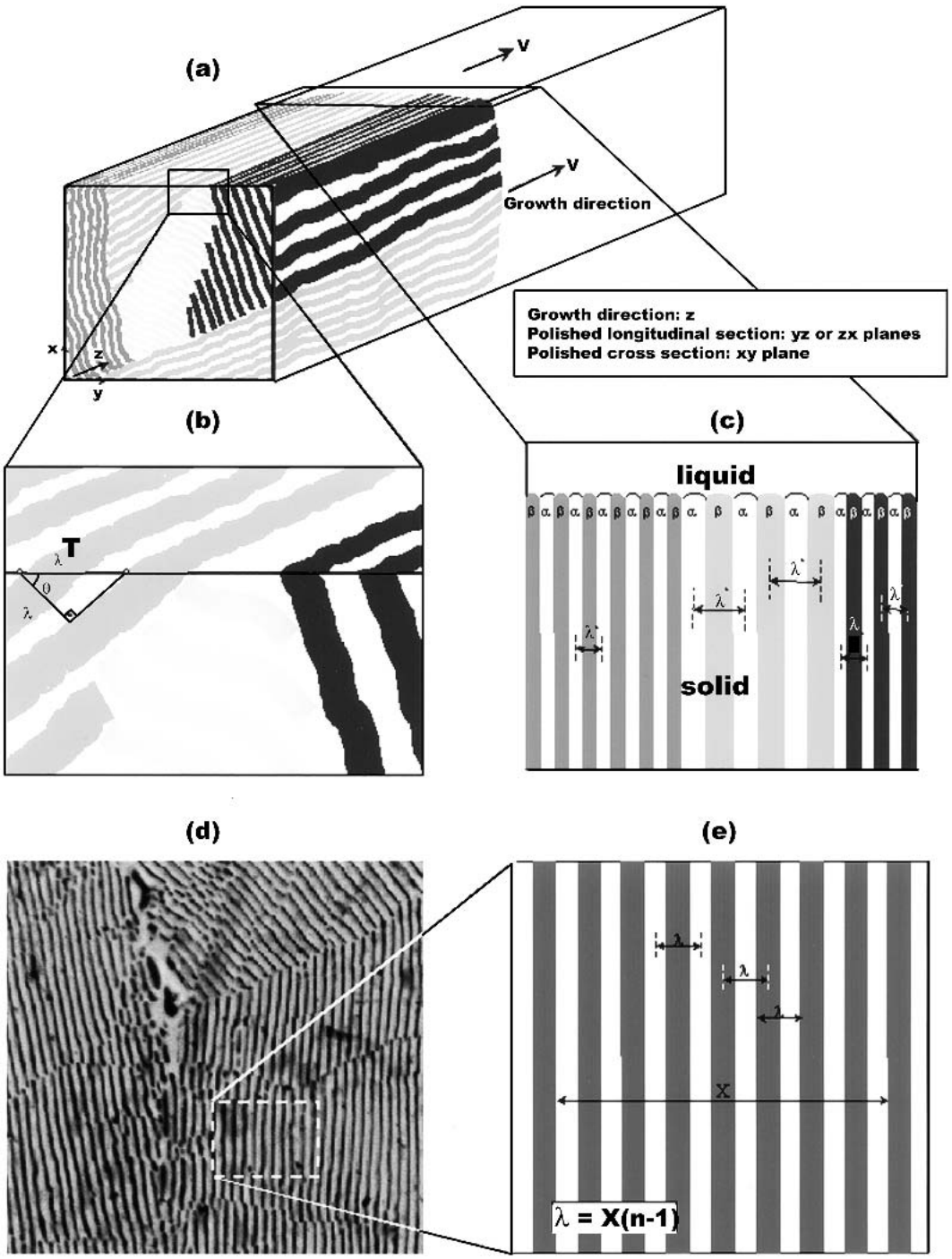

Fig. 2 Schematic illustration of the lamellar spacings measurements on the longitudinal and transverse sections

2.2 Metallographic Examination

The unidirectionally grown quenched specimen was removed from the graphite crucible, then ground to observe the solid-liquid interface, and a longitudinal section that included the quenched interface was separated from the specimen. Thereafter, a transverse and longitudinal section of the specimen was cut from the samples, and it was cold-mounted with epoxy-resin. Then, the samples were wet ground down to grid 2500 and thereafter mechanically polished down with 6, 3, 1, and 1/4 μm diamond paste. Finally the specimen was etched in a solution of 80 ml glycerol, 10 ml nitric acid, and 10 ml acetic acid between 120-180 s.

The microstructure of the specimen was investigated by a light microscope (Olympus, BH-2, Olympus America Inc., Melville, NY) (Fig. 2-5), and scanning electron microscopy (LEO-l, Thornwood, NY) was used to investigate the fine eutectic structures (Fig. 5).

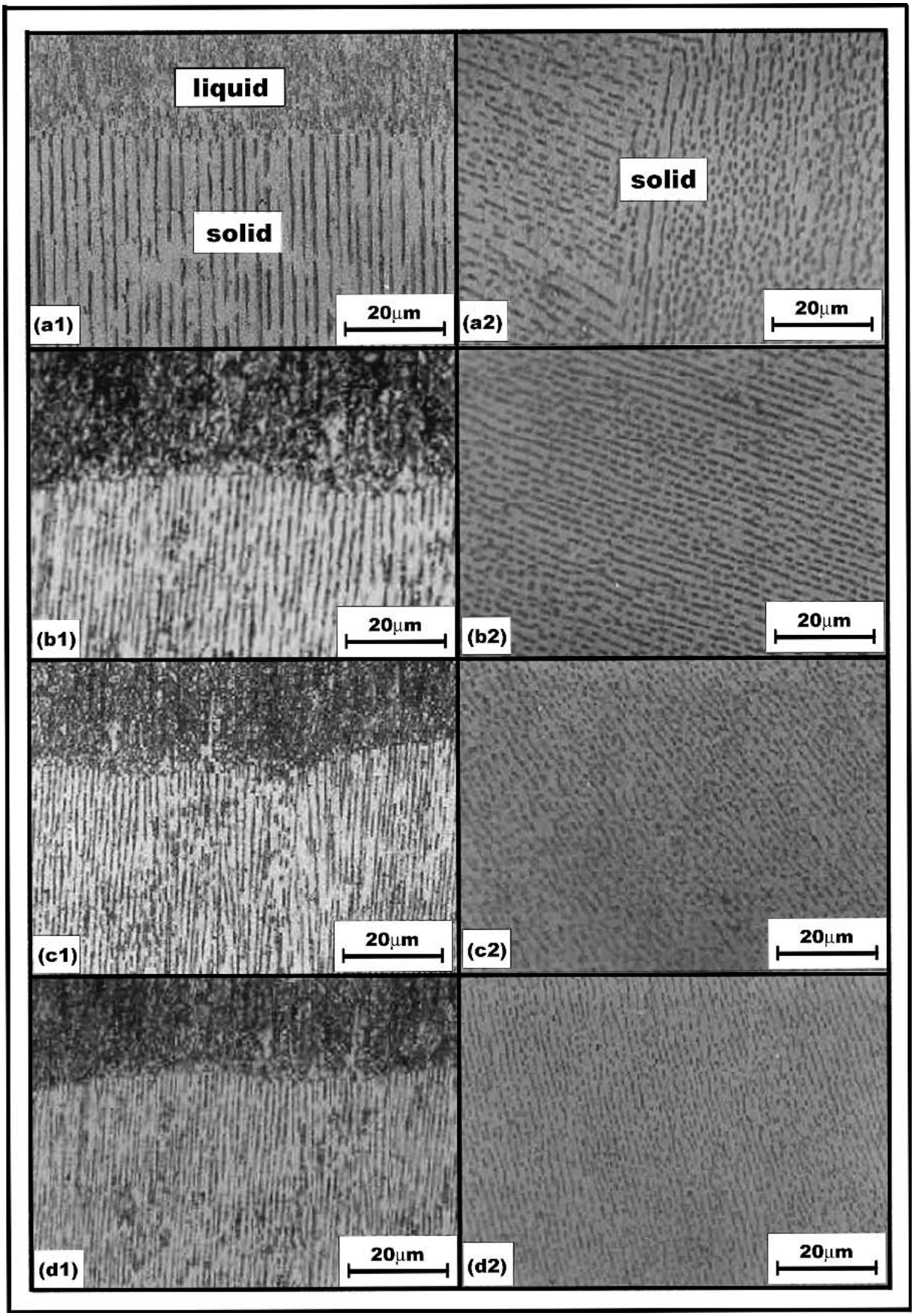

Fig. 3 Variation of lamellar spacings at the constant G (6.52 K/mm) and different V of the directionally solidified Sn-Zn eutectic alloys: **(a_1)** longitudinal section, **(a_2)** transverse section ($V = 16.32$ μm/s), **(b_1)** longitudinal section, **(b_2)** transverse section ($V = 41.48$ μm/s), **(c_1)** longitudinal section, **(c_2)** transverse section ($V = 81.96$ μm/s), **(d_1)** longitudinal section, **(d_2)** transverse section ($V = 165.13$ μm/s)

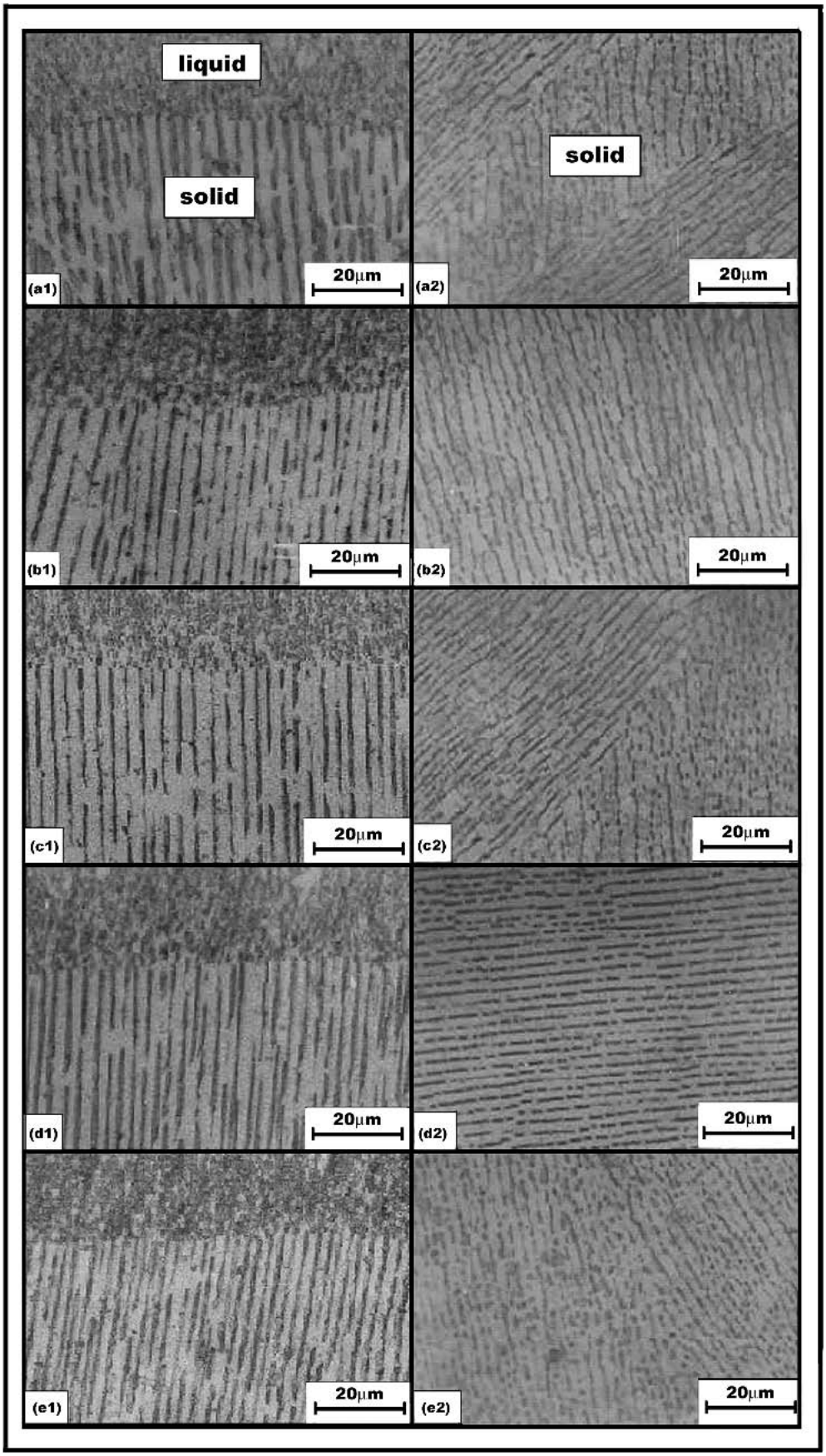

Fig. 4 Variation of lamellar spacings at the constant V (8.33 μm/s) and different G at the directionally solidified Sn-Zn eutectic alloy: **(a_1)** longitudinal section, **(a_2)** transverse section (G = 1.86 K/mm), **(b_1)** longitudinal section, **(b_2)** transverse section (G = 2.97 K/mm), **(c_1)** longitudinal section, **(c_2)** transverse section (G = 4.25 K/mm), **(d_1)** longitudinal section, **(d_2)** transverse section (G = 5.43 K/mm), **(e_1)** longitudinal section, **(e_2)** transverse section (G = 6.52 K/mm)

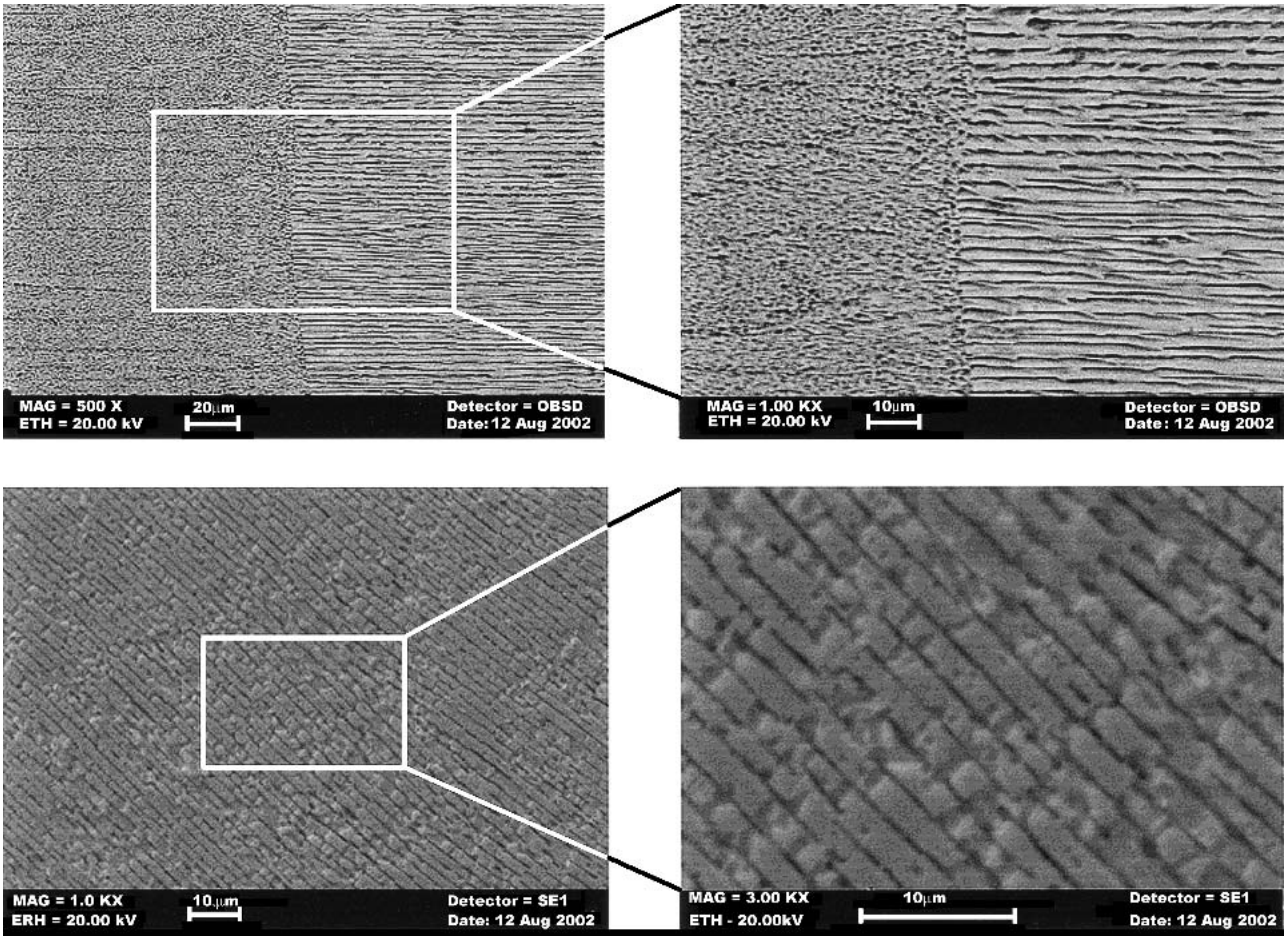

Fig. 5 Scanning electron micrographs of the directionally solidified Sn-Zn eutectic alloy

2.3 The Measurement of Lamellar Spacing λ

The lamellar spacings were measured by metallographic observation on both longitudinal and transverse sections of the samples, about 5 mm behind the quenched interface to ensure being in the steady-state region. The average spacing was obtained from many measurements (typically over 400 lamellar spacings for transverse section) in various representative areas of the sample. These measurements were carried out perpendicular to the general direction of the lamellae in very carefully selected regions where the latter is more or less kept constant over some area within the grains. As can be seen from Fig. 2 during eutectic growth, a large number of eutectic grains with different growth directions can be formed. Thus, in a longitudinal view the lamellar spacing seems to be different in each grain because the grains were cut under different angles. Therefore, the lamellar spacing values of the longitudinal sections often show discrepancy with the measured ones. For this reason, longitudinal sections are inadequate for evaluation of the lamellar spacing. Each grain possessed the crystallographic orientation parallel to growth direction but differed in rotation about the growth axis. Within each grain, well-aligned equally spaced lamellar structure was observed. In addition to the above microstructural characteristics, several growth defects (solidification faults) like layer mismatches and lamellar terminations were observed within each grain.

Approximately 400-500 transverse lamellar spacings λ_a and 50-150 longitudinal lamellar spacings λ_a^* were measured at least in 20 different regions on the transverse section and at least in 4-6 different regions on the longitudinal section of each sample. As can be seen from Fig. 3 and 4, lamellar spacing was measured with a linear intercept method.[28] For the statistical reliability a lot of measurements were taken. The average values of λ_a, λ^*_a, λ^*_m, and λ^*_M were obtained from the detailed measurements (Table 1 and Appendix B, C). The extremum spacing λ_e was obtained from Eq 2a. To make accurate λ measurements from the longitudinal polished plane, the normal of the α and β planes must be parallel to the polished surface; however, this is not always possible. The observed lamellar spacing λ_a^* on the longitudinal plane will be quite different from the lamellar spacings λ_a, observed on the transverse section. The relationship between λ and λ* can be expressed as (Fig. 2)

$$\lambda_a = \lambda^*_a \cos \theta \qquad \text{(Eq 8)}$$

where θ is the angle between the polished longitudinal plane and the normal of the α and β planes. The lamellar spacing obtained from the longitudinal sections is given in Appendix B and C. The undercooling values ΔT_e were obtained from Eq 2c by using the experimental λ, *V*, and *G* values.

Table 1a Case 1 (Constant *G*, Different *V*)

Solidification Parameters			Lamellar Spacings	
G (K/mm)	*V* (μm/s)	ΔT_e (a) (K)	λ_e(b) (μm)	λ_a (μm)
6.52	8.33	0.246	2.11	2.16 ± 0.2
6.52	16.32	0.335	1.51	1.57 ± 0.1
6.52	41.48	0.549	0.94	0.98 ± 0.1
6.52	81.96	0.772	0.67	0.70 ± 0.09
6.52	165.13	1.096	0.47	0.53 ± 0.2
Relationships				
V		$\Delta T_e = k_1 V^{0.50}$	$\lambda_e = k_2 V^{-0.50}$	$\lambda_a = k_3 V^{-0.48}$

Constant (k)	Correlation coefficients (*r*)
$k_1 = 0.09$ (K $\mu m^{-0.50}$ $s^{0.50}$)	$r_1 = 0.999$
$k_2 = 5.32$ ($\mu m^{1.50}$ $s^{-0.50}$)	$r_2 = -0.992$
$k_3 = 5.39$ ($\mu m^{1.48}$ $s^{-0.48}$)	$r_3 = -0.998$

(a) Calculated from Eq 2c
(b) Calculated from Eq 2a

Table 1b Case 2 (Constant *V*, Different *G*)

Solidification Parameters		Lamellar Spacing
G (k/mm)	V (μm/s)	λ_a (μm)
1.86	8.30	3.05 ± 0.2
2.97	8.32	2.82 ± 0.2
4.25	8.27	2.51 ± 0.1
5.43	8.38	2.34 ± 0.2
6.52	8.33	2.16 ± 0.2
Relationship		
G		$\lambda_a = k_4 G^{-0.28}$

Constant (k)	Correlation coefficients (*r*)
$k_4 = 0.52$ ($\mu m^{0.72}$ $K^{0.28}$)	$r_4 = -0.982$

3. Results and Discussion

Sn-8.9 wt.%Zn eutectic samples were solidified with a constant temperature gradient, but five different growth rates, and then with a constant growth rate, but five different temperature gradients, to study the dependence of λ on *V* and ΔT_e and to find the relationship between them.

Lamellar spacings were measured from Fig. 2 and 3 (lamellar spacing for the transverse section λ_a and lamellar spacings for longitudinal section λ_a*, λ^*_m, and λ^*_M). As can be seen in Fig. 3 and 4, the microstructure became finer with increasing both growth rates and temperature gradients. The measurement of the lamellar spacing parameters (microstructure parameters) λ_e, λ_a, λ_a*, λ^*_m, and λ^*_M on the Sn-Zn eutectic alloy are listed in Table 1 and Appendix B and C. Experimental results are presented graphically in Fig. 6(a-c). In Fig. 6(a), log *V* is plotted against log λ for constant *G,* and in Fig. 6(c) log *G* is plotted against log λ for constant *V*.

As can be seen from Fig. 6, the data form straight lines (the linear regression analysis). The relationship between lamellar spacing and solidification parameters was obtained by the linear intercept method.[29] The results are given in Tables 2a and 2b. As can be seen from Table 1 and Appendix B and C, the values of λ_e, λ_a, λ_a*, λ^*_m, and λ^*_M for both sections decrease exponentially as the values of *V*, *G*, and ΔT_e increase.

As can be seen from Fig. 6(a), and Table 1a, the data form straight lines, and the linear regression analysis gives the proportionality equation as

$$\lambda = k V^{-m} \quad \text{(for the constant G)} \qquad \text{(Eq 9)}$$

where k is proportionality constant and given in Table 1a. As can be seen from Tables 1a, 2a, and Appendix B and C, the dependence of the lamellar spacings (λ_e, λ_a, λ_a*, λ^*_m, and λ^*_M) on the growth rate exponent m is equal to 0.50, 0.48, 0.42, 0.43 and 0.36, respectively. It is apparent that the dependence of the microstructural parameters on the growth rate exponent ($\overline{m} = 0.44 \pm 0.04$) was found to be close to the value predicted by theoretical value (0.50) (Eq 2a). The experimental measurements in the Sn-Zn eutectic system obey the relationships $\lambda^2 V$ = constant for a constant *G:*

$$(\lambda_e^2 V = 37.14 \pm 0.30\ \mu m^3/s \text{ (calc.)} \qquad \text{(Eq 10a)}$$

$$\lambda_a^2 V = 40.61 \pm 3.42\ \mu m^3/s \quad \text{(for transverse section)} \qquad \text{(Eq 10b)}$$

$$\lambda^{*2}_a V = 61.57 \pm 10.56\ \mu m^3/s \quad \text{(for longitudinal section)} \qquad \text{(Eq 10c)}$$

$$\lambda^{*2}_m V = 49.2 \pm 8.9\ \mu m^3/s, \quad \text{(for longitudinal section)} \qquad \text{(Eq 10d)}$$

$$\lambda^{*2}_M V = 197.50 \pm 49.22\ \mu m^3/s \quad \text{(for longitudinal section)} \qquad \text{(Eq 10e)}$$

A significant aspect of eutectic growth under the directional solidification condition is the relationship between the growth rate *V* and lamellar spacing λ. According to the J-H model,[11]

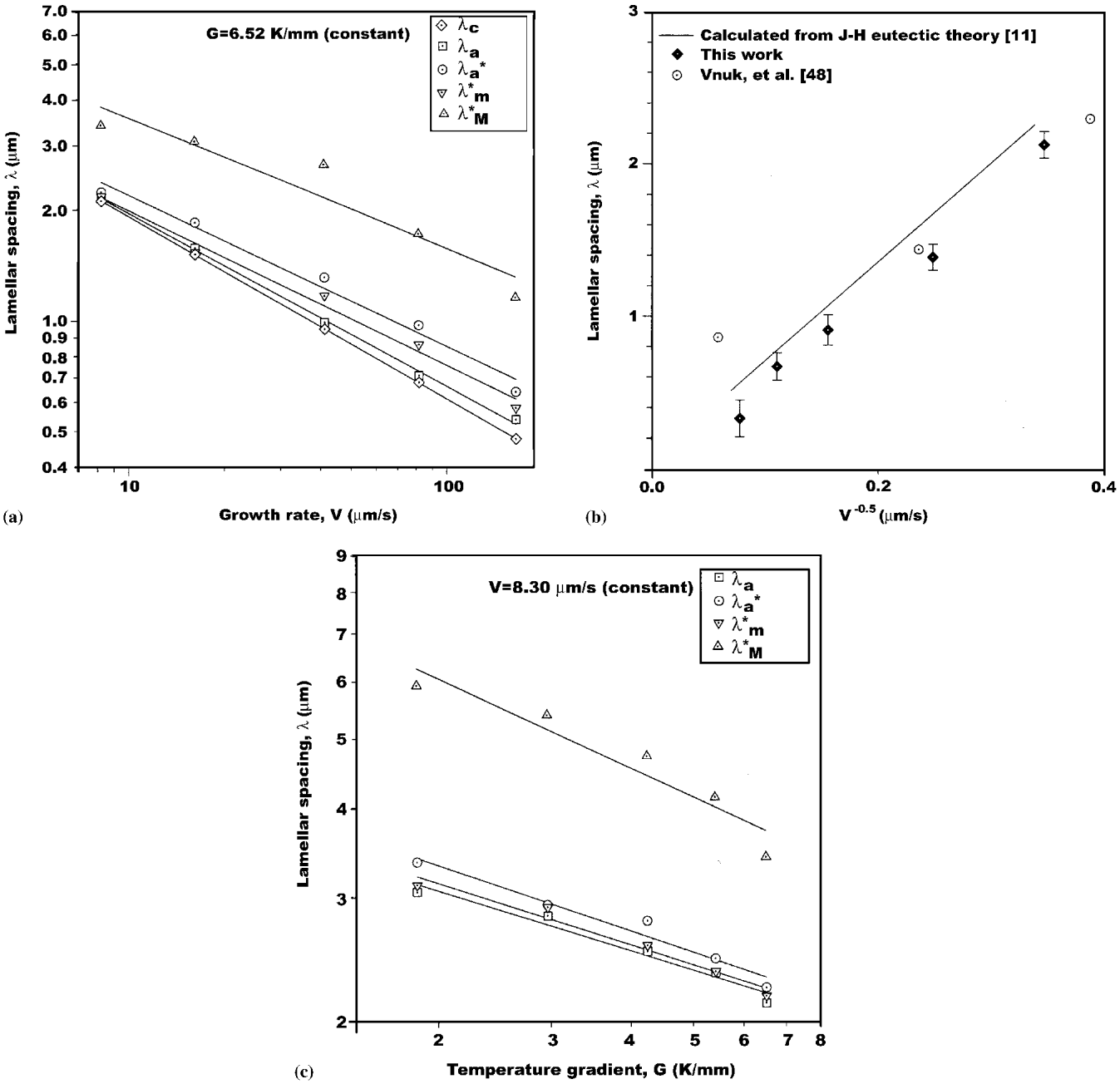

Fig. 6 **(a)** Variation of lamellar spacing λ with growth rates V at a constant temperature gradient (G = 6.52 K/mm), **(b)** variation of the lamellar spacing with growth rate in the Sn-Zn alloy and comparison with obtained values from Jackson-Hunt eutectic theory and experimental data available in the literature (the $\lambda^2 V$ value, which is given in Ref 47 obtained from graphics of the authors), **(c)** variation of lamellar spacing λ with temperature gradients G at a constant growth rate (V = 8.3 μm/s)

the relationship between the inverse square root of the growth rate V and lamellar spacing λ is linear, and generally, experimental results obey the above relationships. In Fig. 6(b) lamellar spacing λ is fitted by linear regression against the inverse square root of the growth rate V. It can be observed that a decrease in growth rate leads to an increase in the lamellar spacing, which means that the relationship $\lambda^2 V$ = constant holds in this system as well. The $\lambda_a^2 V$ (40.61 ± 3.42 $\mu m^3/s$) values of the present work for the transverse section are in good agreement with experimental result 36.4 $\mu m^3/s$, which was obtained by Vnuk et al.,[47] and 37.14 ± 0.112 $\mu m^3/s$, which was obtained by J-H eutectic theory.[11]

As can be seen from Eq 10(d), $\lambda^{*2}_m V$ values for the longitudinal section are greater than the $\lambda_M^2 V$ values for the transverse section. That means λ values for the longitudinal section cannot be used for the theoretical calculations and comparisons with the previous work without geometrical corrections. $\lambda \Delta T_e$ values are given in Table 2a.

Table 2a Case 1 (Constant *G*, Different *V*)

Dependence of λ on ΔT_e, *V*, and *G*								Dependence of ΔT_e on *V*
G (K/mm)	*V* (μm/s)	$\lambda_e \Delta T_e$ (K μm)	$\lambda_a \Delta T_e$ (K μm)	$\lambda_e^2 V$ (μm^3/s)	$\lambda_a^2 V$ (μm^3/s)	$\lambda_e^3 G$ (K μm^2)	$\lambda_a^3 G$ (K μm^2)	$\Delta T_e V^{-0.50}$ # (K $\mu m^{-0.50}$ $s^{0.50}$)
6.52	8.33	0.519	0.531	37.098	38.864	0.0612	0.0657	0.085
6.52	16.32	0.469	0.525	37.112	40.227s	0.0224	0.0252	0.083
6.52	41.48	0.516	0.538	37.272	37.436	0.0054	0.0061	0.085
6.52	81.96	0.517	0.540	36.975	40.160	0.0020	0.0022	0.085
6.52	165.1	0.515	0.581	37.224	46.385	0.0007	0.00010	0.085
		0.507 ± 0.022	0.529 ± 0.036	37.14 ± 0.112	40.614 ± 3.42	λ^3G: is not constant (Fig. 8a)		0.085 ± 0.001

#, obtained from measured V values and calculated ΔT_e values

Table 2b Case 2 (Constantly *V* Different *G*)

G (K/mm)	*V* (μm/s)	$\lambda_a^2 V$ Values (μm^3/s)	$\lambda_a^3 G$ Values (K μm^2)
1.86	8.30	77.21	0.0528
2.97	8.32	66.16	0.0666
4.25	8.27	52.10	0.0672
5.43	8.38	45.89	0.0696
6.52	8.33	37.44	0.0657
		$\lambda_a^2 V$: is not constant (Fig. 8b)	0.0644 ± 0.007

$$\lambda_e \Delta T_e = 0.507 \pm 0.022, \quad \text{(theoretical)} \qquad \text{(Eq 11a)}$$

$$\lambda_a \Delta T_e = 0.529 \pm 0.076 \quad \text{(experimental)} \qquad \text{(Eq 11b)}$$

As can be seen Eq 11, experimental $\lambda_a \Delta T_e$ value is in good agreement with the theoretical $\lambda_e \Delta T_e$ value. The influence of temperature gradient *G* on λ has not been considered in theoretical studies. The influence of *G* cannot be ignored for regular or irregular eutectic systems. The temperature gradient can then influence the lamellar spacings. The influence of temperature gradient on the lamellar spacings was investigated by several authors.[37,48-50] The variation of the lamellar spacings (λ_e, λ_a, λ_a^*, λ^*_m, and λ^*_M) as a function of the temperature gradients is given in Fig. 6(c). It can be observed that an increase in the temperature gradient leads to decrease in the lamellar spacings for a given constant growth rate as well. As a result, $\lambda^2 V$ is no longer constant, i.e., λ decreases with the increasing *G* for a constant *V* (Table 1b). It can be seen that the points fall on a family of straight lines. Thus we can describe the mathematical relationship between λ and *G* by linear regression analysis as

$$\lambda = k\, G^{-n} \text{ (for the constant V)} \qquad \text{(Eq 12)}$$

where k is proportionality constant and given in Table 1b and Appendix B and C. As can be seen from Tables 1b and 2b and Appendix B and C, the dependence of the lamellar spacings (λ_a, λ_a^*, λ^*_m, and λ^*_M) on the temperature gradient exponent n are equal to 0.28, 0.31, 0.29, and 0.42, respectively. The exponent value (0.28) obtained for the transverse section in this work is in good agreement with the result (1/3) obtained by Çadırlı et al.[34] for Al-Cu eutectic alloy and Toloui and Hellawell[48] for Al-Si eutectic alloy. The best approximations would appear to be $\lambda \alpha\ G^{-0.28}$ for the transverse section, and with experimental error in measuring λ and *G*, the results can be summarized for the broken-lamellar structure by $\lambda = kG^{-1/3}$, where k is a constant.

The growth rate, undercooling, and spacing relationship of a eutectic shows the well-known behavior with a minimum undercooling at some characteristic (extremum) spacing (Fig. 7a). The main point of interest here is the operating range, being the range of spacings observed under a given solidification condition.

Figure 7(a) shows numerically predicted variations in the interface undercooling Δ*T* with the lamellar spacings λ for constant *G* (case 1). The extremum undercooling ΔT_e of the solidifying interface was obtained from Eq 2c. ΔT_e-λ curves (Fig. 7a) were plotted by using the experimental *V* values with Eq 2. Figure 7(a) allows accurate $\Delta T_{e \text{ and }} \lambda_e$ data to be obtained for different *V* values by using the higher magnification views of the extremum undercoolings, which are presented in the inset. Figure 7(a) shows the relationship between ΔT_e and λ for the Sn-Zn eutectic system at different growth rates *V* in a constant temperature gradient *G*. As can be seen from Fig. 7(a), ΔT_e increases with the increasing growth rate as the extremum spacing λ_e decreases. As can be seen in Table 1 and Fig. 6(a and b), the influence of *V* is certain on the lamellar spacing λ and ΔT_e. The values of *V* increased approximately 20 times, ΔT_e values increased 4 times, *G* values increased 3.5 times, and ΔT_e values increased 1.7 times. The influence of *V* was more effective then G. Figure 7(b) shows the variation of undercoolings ΔT_e increases with increasing *V*. As can be seen from Tables 1 and 2 and Fig. 7(b), the dependence of ΔT_e on *V* and λ_e can be given as

$$\Delta T_e = k_1\, V^{0.50}, \ (k_1 = 0.085 \text{ K } \mu m^{-0.50} s^{0.50}) \qquad \text{(Eq 13a)}$$

$$\lambda_e\, \Delta T_e = 0.507 \pm 0.022 \ \mu m.K \qquad \text{(Eq 13b)}$$

The exponent value 0.50 is equal to the theoretical value (0.50) (Eq 2c).

Figures 8(a and b) show the variation of $\lambda^3 G$, as function of growth rate for constant *G* and the variation of $\lambda^2 V$ as function of temperature gradient for constant *V*, respectively. The values of λ^3G decrease as the values *V* increase (Fig. 8a)

$$\lambda_e^3 G = k_1\, V^{-1.50} \ (k_1 = 1.457\ \mu m^{3.5} \text{ K } s^{-1.50}) \qquad \text{(Eq 14a)}$$

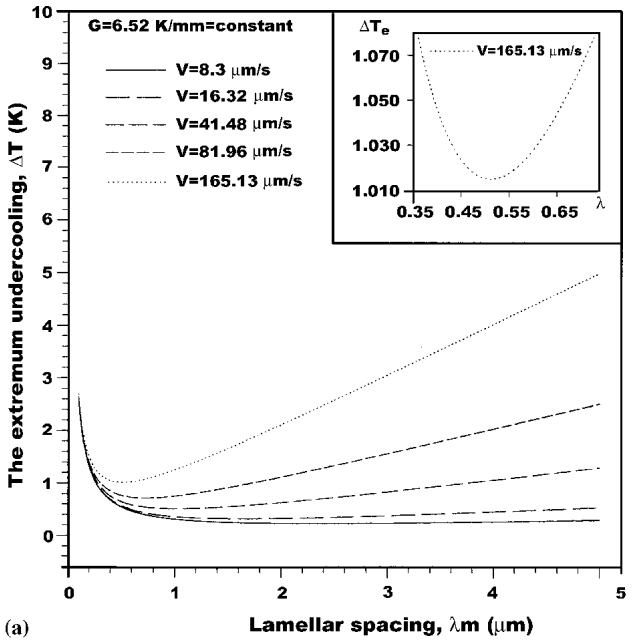

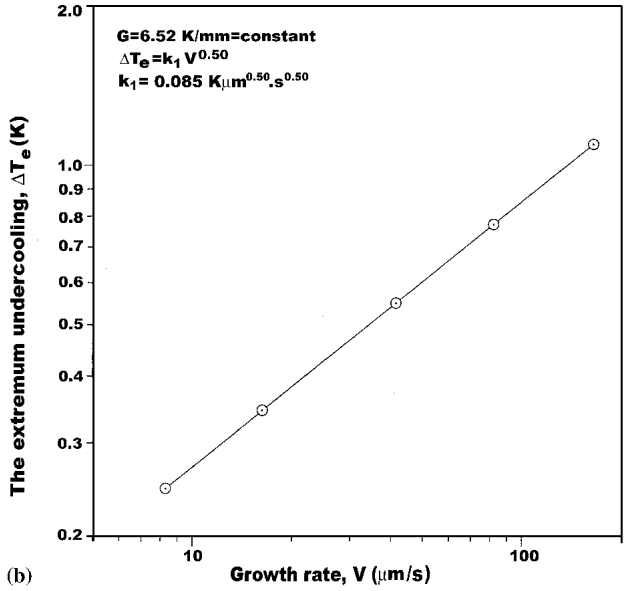

Fig. 7 **(a)** Variation of the calculated extremum ΔT with the lamellar spacing λ at a constant temperature gradients G (6.52 K/mm) (higher magnification views of the minimum undecoolings are presented in the inset); **(b)** variation of the extremum undercooling ΔT as function of V at a constant G (6.52 K/mm)

$$\lambda_a^3 G = k_2 V^{-1.43} \quad (k_2 = 1.288\ \mu m^{3.43}\ K\ s^{-1.43}) \qquad \text{(Eq 14b)}$$

$$\lambda_e^{3*} G = k_3 V^{-1.27} \quad (k_3 = 1.292\ \mu m^{3.27}\ K\ s^{-1.27}) \qquad \text{(Eq 14c)}$$

From Eq 14, λ_a can be expressed as follows:

$$\lambda_a = k' V^{-1/2} G^{-1/3} \qquad \text{(Eq 14d)}$$

and the values of $\lambda^2 V$ decrease as the values G increase (Fig. 8b).

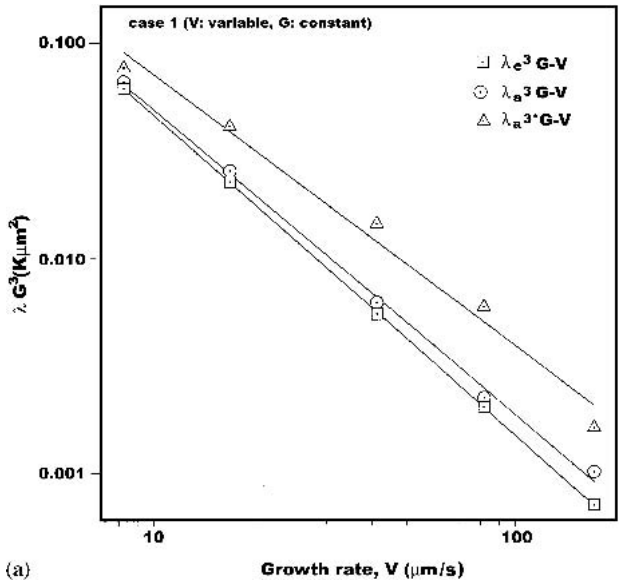

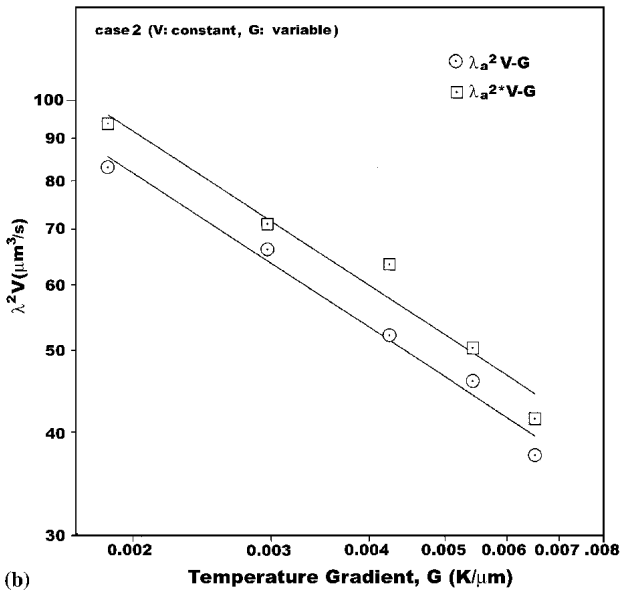

Fig. 8 **(a)** Variation of $\lambda^3 G$, as a function of V at a constant G; **(b)** variation of the bulk growth rate, $\lambda^2 V$, as a function of G at a constant V

Appendix A
Physical Parameters Used for Sn-Zn Eutectic Alloy

T_E (K)	569[46]
m_α K (wt.%)$^{-1}$	−3.82[46]
m_β K (wt.%)$^{-1}$	2.43[46]
C_E (wt.%)	8.9[46]
C^*_o (wt.%)	97.48[46]
f_α	0.917[7]
f_β	0.083[7]
Γ_α (K μm)	0.102[51]
Γ_β (K μm)	0.048[51]
θ_α (°)	18.43[51]
θ_β (°)	19.25[51]
D (μm^2/s)	3500[52]
K_1 (K s/μm^2)	0.007 (calculated from the physical parameters)
K_2 (K μm)	0.260 (calculated from the physical parameters)

Appendix B

Table B1 Case 1 (Constant *G*, Different *V*)

Solidification Parameters			Lamellar Spacings					
G, K/mm	V, μm/s	ΔT_e (a), K	θ, °	λ_e, (b) μm	λ_a, μm	λ_a*, μm	λ_m*, μm	λ_M*, μm
6.52	8.33	0.246	14.394	2.11	2.16 ± 0.2	2.23 ± 0.2	2.17 ± 0.25	3.40 ± 0.40
6.52	16.32	0.335	31.432	1.51	1.57 ± 0.1	1.84 ± 0.1	1.53 ± 0.21	3.06 ± 0.33
6.52	41.48	0.549	41.075	0.94	0.98 ± 0.1	1.30 ± 0.2	1.16 ± 0.14	2.63 ± 0.22
6.52	81.96	0.772	43.183	0.67	0.70 ± 0.09	0.96 ± 0.1	0.85 ± 0.08	1.70 ± 1.14
6.52	165.1	1.096	37.725	0.47	0.53 ± 0.2	0.63 ± 0.08	0.57 ± 0.07	1.14 ± 0.06
Relationships								
V		$\Delta T_e = k_1 V^{0.50}$		$\lambda_e = k_2 V^{-0.50}$	$\lambda_a = k_3 V^{-0.48}$	$\lambda_a^* = k_4 V^{-0.42}$	$\lambda_m^* = k_5 V^{-0.43}$	$\lambda_M^* = k_6 V^{-0.36}$

Constant (k)	Correlation Coefficients (*r*)
$k_1 = 0.09$ (K μm$^{-0.50}$ s$^{0.50}$)	$r_1 = 0.999$
$k_2 = 5.32$ (μm$^{1.50}$ s$^{-0.50}$)	$r_2 = -0.992$
$k_3 = 5.39$ (μm$^{1.48}$ s$^{-0.48}$)	$r_3 = -0.998$
$k_4 = 5.75$ (μm$^{1.42}$ s$^{-0.42}$)	$r_4 = -0.991$
$k_5 = 5.34$ (μm$^{1.43}$ s$^{-0.43}$)	$r_5 = -0.994$
$k_6 = 8.128$ (μm$^{1.36}$ s$^{-0.36}$)	$r_6 = -0.954$

(a) Calculated from Eq 2c
(b) Calculated from Eq 2a

Table B2 Case 2 (Constant *V*, Different *G*)

Solidification Parameters		Lamellar Spacings				
G, K/mm	*V*, μm/s	θ, °	λ_a, (a) μm	λ_a* (b), μm	λ_m*, μm	λ_M*, μm
1.86	8.30	24.805	3.05 ± 0.2	3.36 ± 0.2	3.12 ± 0.51	5.92 ± 0.92
2.97	8.32	15.038	2.82 ± 0.2	2.92 ± 0.1	2.90 ± 0.46	5.38 ± 0.77
4.25	8.27	25.023	2.51 ± 0.1	2.77 ± 0.2	2.56 ± 0.30	4.71 ± 0.71
5.43	8.38	17.234	2.34 ± 0.2	2.45 ± 0.2	2.35 ± 0.26	4.12 ± 0.51
6.52	8.33	14.394	2.16 ± 0.2	2.23 ± 0.2	2.17 ± 0.21	3.40 ± 0.58
Relationships						
G			$\lambda_a = k_7 G^{-0.28}$	$\lambda_a^* = k_8 G^{-0.31}$	$\lambda_m^* = k_9 G^{-0.29}$	$\lambda_M^* = k_{10} G^{-0.42}$

Constant (k)	Correlation Coefficients (r)
$k_7 = 0.52$ (μm$^{0.72}$ K$^{0.28}$)	$r_7 = -0.982$
$k_3 = 0.48$ (μm$^{0.69}$ K$^{0.31}$)	$r_8 = -0.980$
$k_9 = 0.51$ (μm$^{0.71}$ K$^{0.29}$)	$r_9 = -0.983$
$k_{10} = 0.45$ (μm$^{0.58}$ K$^{0.42}$)	$r_{10} = -0.954$

(a) Values of the lamellar spacing obtained from the transverse section of the samples
(b) Values of the lamellar spacing obtained from the longitudinal section of the samples

Table C1
Case 1 (Constant *G*, Different *V*)

Dependence of λ on ΔT_e, *V*, and *G*									Dependence of ΔT_e on *V*
$\lambda_e \Delta T_e$, K μm	$\lambda_a \Delta T_e$, K μm	$\lambda_a^* \Delta T_e$, K μm	$\lambda_e^2 V$, μm^3/s	$\lambda_a^2 V$, μm^3/s	$\lambda_a^{2*} V$, μm^3/s	$\lambda_e^3 G$, K μm^2	$\lambda_a^3 G$, K μm^2	$\lambda_a^{3*} G$, Kμm^2	$\Delta T_e V^{-0.50}$ (a), K μm$^{-0.50}$s$^{0.50}$
0.519	0.531	0.549	37.098	38.864	41.42	0.0612	0.0657	0.0723	0.085
0.469	0.525	0.616	37.112	40.227s	55.25	0.0224	0.0252	0.0406	0.083
0.516	0.538	0.714	37.272	37.436	70.10	0.0054	0.0061	0.0143	0.085
0.517	0.540	0.741	36.975	40.160	75.53	0.0020	0.0022	0.0058	0.085
0.515	0.581	0.691	37.224	46.385	65.54	0.0007	0.00010	0.0016	0.085
0.507 ± 0.022	0.529 ± 0.036	0.662 ± 0.076	37.14 ± 0.112	40.614 ± 3.42	61.57 ± 10.56				0.085 ± 0.001
($\lambda_m^* \Delta T_e = 0.571 \pm 0.038$)			($\lambda_m^{2*} V = 49.20 \pm 8.91$)			$\lambda^3 G$ is not constant (Fig. 8a)			
($\lambda_M^* \Delta T_e = 1.127 \pm 0.182$)			($\lambda_M^{2*} V = 197.50 \pm 49.22$)						
			$\lambda_e^2 W = 37.14$ (calc. Eq 2a)						

(a) Calculated from Eq 2c.

Table C2 Case 2 (Constant *V*, Different *G*)

λ^2 *V* Values				λ^3 G Values			
$\lambda_a^2 V$ ($\mu m^3/s$)	$\lambda_a^2{}^* V$ ($\mu m^3/s$)	$\lambda_m^2{}^* V$ ($\mu m^3/s$)	$\lambda_m^2 V$ ($\mu m^3/s$)	$\lambda_a^3 G$ (K μm^2)	$\lambda_a^3{}^* G$ (K μm^2)	$\lambda_m^3{}^* G$ (K μm^2)	$\lambda_M^3{}^* G$ (K μm^2)
77.21	93.70	80.79	290.89	0.0528	0.0706	0.0565	0.3859
66.16	70.94	69.97	240.82	0.0666	0.0739	0.0724	0.4625
52.10	63.45	54.19	183.46	0.0672	0.0903	0.0713	0.4441
45.89	50.30	46.28	142.25	0.0696	0.0799	0.0705	0.3797
37.44	41.42	39.225	96.295	0.0657	0.0723	0.0666	0.2563
	$\lambda_e^2 V$: is not constant (Fig 8b)			0.0644 ± 0.007	0.0774 ± 0.0080	0.0675 ± 0.0065	0.3857 ± 0.0808

$$\lambda^2 V = k'' G^{-0.63} \quad (k'' = 1.775\ K^{0.63}\ \mu m^{2.37} s^{-1}) \qquad \text{(Eq 15a)}$$

$$\lambda_a^{2*} V = k'' G^{-0.62} \quad (k'' = 1.993\ K^{0.62}\ \mu m^{2.38} s^{-1}) \qquad \text{(Eq 15b)}$$

As can be seen from Eq 14b and 15a, λ_a values decrease with increasing *G* and *V* values.

The average value of exponents (0.63) in this work is in good agreement with those obtained by Toloui and Hellawell (0.67)[48] for Al-Si eutectic alloy, Fisher and Kurz (0.81)[53] for Al-Si eutectic alloy, Schürman and Löblich (0.7)[54,55] for cast iron, and Fisher (0.84)[56] for borneol-succinonitrile.

4. Conclusions

The broken-lamellar spacings were measured from the transverse section λ and the longitudinal section λ^* of the directionally solidified Sn-Zn eutectic samples. It was seen that λ is more reliable than λ^*. The reason for this might be that λ is perpendicular to the growth direction, whereas λ^* depends on the polished plane.

The change of the lamellar spacings (λ_a^*, λ_a, λ^*_e, λ^*_m, and λ^*_M), according to the solidification parameters *V*, *G*, and ΔT for the Sn-Zn eutectic alloy, was investigated and relationships between them were obtained by the intercept method. It shows that the value of the lamellar spacing decreases as the values of *V*, *G*, and ΔT increase. The experimentally obtained $\lambda_a^2 V = 40.61\ \mu m^3/s$ value is in good agreement with the theoretical value $\lambda_e^2 V = 37.14\ \mu m^3/s$ and the experimentally value 36.4 $\mu m^3/s$, which was obtained by Vnuk et al.[34] for the similar *G* and *V* values. $\lambda^2 V$ values decrease with the increasing *G* values for a given *V*.

$\lambda_a^3 G$, $\lambda_a^{3*} G$, $\lambda_m^3 G$ and $\lambda_M^{3*} G$ values have been found to be constant for a given *V*, but $\lambda^3 G$ values decrease with the increasing *V* for a given *G*.

Effects of growth rates *V* on the undercooling ΔT_e were examined, and the relationship between *V* and ΔT_e was obtained as follows: $\Delta T_e = k_1 V^{0.50}$ (for case 1). That is, ΔT_e increases with the increasing *V* values.

J-H eutectic theory for the regular eutectic system is also used for the broken-lamellar eutectic growth.

Although experimental variation of *G* is much narrower than the variation of *V*, *G* affects λ in a way similar to *V*. In general, variation of λ with *V* and *G* can be expressed as $\lambda_a = k' V^{-1/2} G^{-1/3}$.

References

1. R.W. Kraft and D.L.A. Albright: "Microstructure of Unidirectionally Solidified Al-$CuAl_2$ Eutectic," *Trans. Met. Soc. AIME,* 1961, *221,* pp. 95-102.
2. H.E. Cline*: Metall. Trans.,* 1971, *2,* p. 189.
3. E.R. Thompson and F.D. Lemkey: *Trans ASM,* 1969, *62,* p. 140.
4. M.F.X. Gigliotti, R. Melvin, F. Michael, A.David, S. Sherwin, and A.Charles: "Transverse Ductile Fiber Reinforced Eutectic Nickel-Base Superalloys," U.S. Patent No. 4 292 076, 1981.
5. R. Caram and S. Milenkovic: "Microstructure of Ni-Ni_3Si Eutectic Alloy Produced by Directional Solidification," *J. Cryst. Growth,* 1999, *198/199,* pp. 844-49.
6. F.S. Galasso: *J. Metals,* 1967, *19,* p. 17.
7. M.N. Crocker, D. Baragar, and R.W. Smith: "Anamolous Eutectic Growth," *J. Cryst. Growth,* 1975, *30,* pp. 198-212.
8. R. Elliot, *Eutectic Solidification Processings,* Butterworths, London, UK, 1983, p. 136.
9. J.M. Liu, Z.G. Liu, and Z.C. Wu: "Spacing Selection for an Sn-Pb Lamellar Eutectic During Directional Solidified," *Mater. Sci. Eng.* 1993, *A167,* p. 87.
10. M.R. Aguiar and R. Caram: "Directional Solidified of a Sn-Se Eutectic Alloy Using the Bridgman-Stockbarer Method," *J. Cryst. Growth,* 1996, *166,* pp. 398-401.
11. K.A. Jackson and J.D. Hunt: "Lamellar and Eutectic Growth," *Trans. Met. Soc. AIME,* 1966, *236,* pp. 1129-42.
12. J.M. Liu: "Dynamics of Spacing Selection of a Lamellar Eutectic During Directional Solidification," *Mater. Sci. Eng.,* 1992, *A157,* pp. 73-78.
13. H.E. Cline: "Strengthening of Lamellar vs Equiaxed Ag-Cu Eutectic," *Acta Metall.,* 1972, *18,* pp. 315-23.
14. R.M. Jordan and J.D. Hunt: "The Growth of Lamellar Eutectic Structures in the Pb-Sn and Al-$CuAl_2$ Systems," *Metall. Trans.,* 1971, *2,* pp. 3401-10.
15. T. Sato and Y. Sayama: "Completely and Partially Co-operative Growth of Eutectic," *J. Cryst. Growth,* 1974, *22,* pp. 259-71.
16. G.E. Nash: "A Self Consistent Theory of Steady State Lamellar Solidification in Binary Eutectic Systems," *J. Cryst. Growth,* 1977, *38,* pp. 155-80.
17. H.E. Cline: "Growth of Eutectic Alloy, Tin Films," *J. Appl. Phys.,* 1979, *50,* p. 4780; *Mater. Sci. Eng.* 1984, *65,* pp. 93-100.
18. J.S. Langer: "Eutectic Solidification," *Phys. Rev. Lett.,* 1980, *44,* p. 1023.
19. V. Dayte and J.S. Langer: "Stability of Thin Lamellar Eutectic Growth," *Phys. Rev. B,* 1981, *24,* p. 4155.
20. D.A. Kessler and H. Levine: "Computational Approach to Steady State Eutectic Growth," *J. Cryst. Growth,* 1989, *94,* p. 871.
21. A. Karma: "Wavelength Selection in Directional," *Phys. Rev. Lett.,* 1986, *57,* p. 858.
22. A. Karma and P. Pelce: "Oscillatory of Deer Cels in Directional Solidification," *Phys. Rev. A,* 1989, *39,* p. 4162.
23. C. Zener: *Trans. AIME,* 1946, *167,* p. 550.
24. V. Seetharaman and R. Trivedi: "Eutectic Growth," *Metall. Trans.,* 1988, *19A,* pp. 2955-64.
25. R. Trivedi, J.T. Mason, J.D. Verhoeven, and W. Kurz: "Eutectic Spac-

ing Selection in Lead-Based Alloy Systems," *Metall. Trans.,* 1991, *22A,* pp. 2523-33.
26. H. Müller-Kurumbhaar and W. Kurz: in *Material Science and Technology: A Comprehensive Treatment,* Vol. 5, R.W. Chan, P. Haasen, and E.J. Kramer, ed., VCH, New York, 1991, p. 554.
27. R. Elliot: "Eutectic Solidification," *Mater. Sci. Eng.,* 1984, *65,* pp. 85-92.
28. S.C. Gill and W. Kurz: "Rapid Solidification Al-Cu Alloys—I. Experiment Determination of the Microstructure Selection MAP," *Acta Metall.,* 1993, *41*(12), pp. 3563-73.
29. A. Ourdjini, J. Liu, and R. Elliott: "Eutectic Spacing Selection in the Al-Cu System," *Mater. Sci. Technol.,* 1994, *10,* pp. 312-18.
30. K.B. Kim, J. Liu, N. Maraşlı, and J.D. Hunt: "The Effect of Different Atomic Volumes in the Three Phases During Lamellar Eutectic Growth. A Comparison of Experiment and Theory in the Al-Al_2Cu System," *Acta Metall.,* 1995, *43*(6), pp. 2143-47.
31. M. Tassa and J.D. Hunt: "The Measurement of Al-Cu Dendrite Tip and Eutectic Interface Temperatures and Their Use for Predicting the Extent of the Eutectic Range," *J. Cryst. Growth,* 1976, *34,* pp. 38-48.
32. E. Çadırlı and M. Gündüz: "The Dependence of Lamellar Spacing on Growth Rate and Temperature Gradient in the Lead-Tin Eutectic Alloy," *J. Mater. Process. Technol.,* 2000, *97,* pp. 74-81.
33. E. Çadırlı, A. Ülgen, and M. Gündüz: "Directional Solidification of the Aluminium-Copper Eutectic Alloy," *Mater. Trans. JIM,* 1999, *40*(9), pp. 989-96.
34. H. Jones and W. Kurz: "Ration of Interphase Spacings and Growth Temperature to Growth Velocity in Fe-C and Fe-Fe_3 Eutectic Alloys," *Z. Metalkd.,* 1981, *72,* pp. 792-97.
35. P. Magnin, J.T. Mason, and R. Trivedi: "Growth of Irregular Eutectics and the Al-Si System," *Acta Metall. Mater.,* 1991, *39,* pp. 469-80.
36. Y.X. Zhuang, X.M. Zhang, L.H. Zhu, and Z.Q. Hu: "Eutectic Spacing and Faults of Directionally Solidified Al-Al_3Ni Eutectic," *Sci. and Tech. Adv. Mater.,* 2001, *2,* pp. 37-39.
37. L.M. Hogan and H. Song: "Interparticle Spacings and Undercooling in Al-Si Eutectic Microstructure," *Metall. Trans.,* 1987, *18A,* pp. 707-13.
38. P. Magnin and W. Kurz: "An Analytical Model of Irregular Eutectic Growth and Its Application to Fe-C," *Acta Metall.,* 1987, *35,* pp. 1119-28.
39. P. Magnin and R. Trivedi: "Eutectic Growth: A Modification of the Jackson–Hunt Theory," *Acta Metall. Mater.,* 1991, *39,* pp. 453-67.
40. P.H. Shingu: *J. Appl. Phys.,* 1979, *50,* p. 5743.
41. Y. Wang, H. Jones, and P. V. Evans: "Eutectic Solidification Characteristics of Bridgman Growth Al-3Fe-0.1V Alloy," *J. Mater. Sci.,* 1998, *33,* pp. 5205-20.
42. M.R. Aguiar and R. Caram: "Lamellar Spacing Selection in a Directional Solidified Sn-Se Eutectic Alloy," *J. Cryst. Growth,* 1997, *174,* pp. 70-75.
43. S. Guldberg and N. Ryum: "Microstructure and Crystallographic Orientation Relationship in Directionally Solidified Mg-$Mg_{17}Al_{12}$-Eutectic," *Mater. Sci. Eng.,* 2000, *A289,* p. 143.
44. M. Gündüz: *The Measurement of the Solid-Liquid Surface Energy,* Ph.D. Thesis, Oxford University, Oxford, UK, 1984, p. 60.
45. D.G. McCartney: *Studies on Cellular and Dendritic Solidification,* Ph.D. Thesis, Oxford University, Oxford, UK, 1981, p. 95.
46. T. Lyman, ed.: *Metals Handbook—Fractograph and Atlas of Fractographs,* Vol. 8, 8th ed., American Society for Metals (ASM Handbook Committee), Metals Park, OH, 1973, p. 336
47. F. Vnuk, M. Sahoo, D. Baragor, and R.W. Smith: "Mechanical Properties of Sn-Zn Eutectic Alloys," *J. Mater. Sci.,* 1980, *15,* pp. 2573-80.
48. B. Toloui and A. Hellawell: "Phase Separation and Undercooling in Al-Si Eutectic Alloy—The Influence of Freezing Rate and Temperature Gradient," *Acta Metall.* 1976, *24,* pp. 565-73.
49. R. Elliott and S.M.D. Glenister: "Strontium Modification of Al-12.7 wt.% Si Alloys," *Metal Sci.,* 1981, *4,* pp. 181-84.
50. S. Li, S. Zhao, M. Pan, D. Zhao, X. Chan, O.M. Barabash, and R.I. Barabash: "Solidification and Structural Characteristics of α (Al)-Mg_2Si Eutectic," *Mater. Trans. JIM,* 1997, *38,* pp. 553-59.
51. B. Saatci: *The Measurement of the Solid-Liquid Surface Energy,* D. Phil. Thesis, University of Erciyes, Kayseri, Turkey, 2000, p. 167.
52. D. Bouchhard and J.S. Kirkaldy: "Prediction of Dendrite Arm Spacings in Unsteady and Steady-State Heat Flow of Unidirectionally Solidified Binary Alloys," *Metall. Mater. Trans.,* 1997, *28B,* pp. 651-63.
53. D.J. Fisher and W. Kurz: "A Theory of Branching Limited Growth of Irregular Eutectics," *Acta Metall.,* 1980, *28,* pp. 777-94.
54. E. Schürman and H. Löblich: *Giessereiforschung,* 1977, *29,* p. 67.
55. E. Schürman and H. Löblich: *43rd Int. Foundry Congress,* Bucharest, 1976, p. 17.
56. D.J. Fisher: Ecole Polytechnique Federale de Lausanne, Sc.D. Thesis, 1978.